Proceedings of the 20th International Conference on Soil Mechanics and Geotechnical Engineering– Rahman and Jaksa (Eds)

Data processing for shear-wave velocity monitoring on geotechnical downhole array

Traitement des données pour la surveillance de la vitesse des ondes de cisaillement sur un réseau géotechnique de fond de puits

Tadahiro Kishida & Deepa Kunhiraman Nambiar
Civil Infrastructure and Environmental Engineering, Khalifa University of Science and Technology, United Arab Emirates, tadahiro.kishida@ku.ac.ae

Chi-Chin Tsai
Department of Civil Engineering, National Chung Hsing University, Taiwan

Chun-Hsiang Kuo
Department of Earth Sciences, National Central University, Taiwan

ABSTRACT: Geotechnical strong-motion downhole arrays provide acceleration times series in depths. The previous studies show that dynamic soil responses are identified by fundamental frequencies of transfer function, shear wave velocities between sensors, and insitu stress-strain curves obtained from recorded acceleration time series. However, there is no study that combines these different monitoring observations to identify the geotechnical dynamic system behaviors. This study integrates these observations to identify the dynamic soil responses at Wildlife Liquefaction Array. Shear wave velocities are obtained by wave travel time between sensors with Normalized Input-Output Method and by generic-algorithm inversion analysis based on transfer functions of horizontal motions. Shear modulus is also computed between sensors by calculating insitu stress-strain time series. Standard deviations are computed throughout these processes. Transitions of dynamic soil responses during strong shaking are identified through joint inversion of the observed data. Moreover, the obtained behavior is assessed with the measured pore water pressure to evaluate the soil-water coupling effect.

RÉSUMÉ : Les réseaux géotechniques de fond de trou à mouvement fort fournissent des séries temporelles d'accélération en profondeur. Les études précédentes montrent que les réponses dynamiques du sol sont identifiées par les fréquences fondamentales de la fonction de transfert, les vitesses des ondes de cisaillement entre les capteurs et les courbes contrainte-déformation in situ obtenues à partir de séries temporelles d'accélération enregistrées. Cependant, il n'existe aucune étude combinant ces différentes observations de surveillance pour identifier les comportements géotechniques du système dynamique. Cette étude intègre ces observations pour identifier les réponses dynamiques du sol à Wildlife Liquefaction Array. Les vitesses des ondes de cisaillement sont obtenues par le temps de parcours des ondes entre les capteurs avec la méthode d'entrée-sortie normalisée et par l'analyse d'inversion d'algorithme générique basée sur les fonctions de transfert des mouvements horizontaux. Les modules de cisaillement sont également calculés entre les capteurs en calculant des séries temporelles de contraintes et de déformations in situ. Les écarts types sont également calculés tout au long de ces processus. Les transitions des réponses dynamiques du sol lors de fortes secousses sont identifiées par l'inversion conjointe de ces données observées. Le comportement obtenu est évalué avec la pression d'eau interstitielle mesurée pour évaluer l'effet de couplage sol-eau.

KEYWORDS: downhole array, shear wave, inversion, liquefaction.

1 INTRODUCTION

Site response analyses compute the amplifications of seismic waves propagating through subsurface soil layers. Effective stress site response analysis can represent the generation of excess pore water pressure and associated cyclic softening of soil under strong shaking (e.g. Hashash et al. 2020). However, numerically predicting the wave propagation, generation and redistribution of excess pore water pressures, and the resulting vertical settlement remains challenging even under relatively simplistic level-ground free-field conditions.

Downhole array data are very useful to understand the dynamic soil behaviors. Dynamic site responses and soil behaviors have been investigated through different techniques. Wave velocities were calculated during strong motions by computing the wave travel times between sensors (Elgamal et al. 1995). Inversion analyses were performed (e.g. Aguirre & Irikura 1997) to identify dynamic soil properties with time. Furthermore, stress–strain behaviors were extracted to understand soil nonlinear behaviors during strong shakings (e.g. Zeghal & Elgamal 1994). Although many methods have been developed to analyze downhole data, the combination of these methodologies to reduce the uncertainties in dynamic soil behaviors have not been studied.

This study analyzes the data from Wildlife Liquefaction Array containing recorded measurements of acceleration and pore water pressure. The Wildlife Station was established by the US Geological survey in 1982 on a floodplain in the Imperial Valley of Southern California, wherein sand boils were developed during the 1981 Westmorland earthquake (Bennett et al., 1984). The station has been operated under United States National Strong-Motion Network (NP) with Station ID of 5210. In 2003-04, the Wildlife Liquefaction Array was instrumented as part of the US National Science Foundation (NSF) Network for Earthquake Engineering Simulation (NEES) (Youd et al., 2007). The station has been operated under UC Santa Barbara Engineering Seismology Network (SB) with Station ID of WLA. These stations are separated by approximately 70 m. These data were previously analyzed and showed reasonable results on the recorded variables (Steidl et al. 2014, Kishida & Tsai 2021). This study calculates shear wave velocity (V_s) during strong motions using Normalized Input-Output Minimization (NIOM) (Haddadi & Kawakami 1998). Shear stress-strain behaviors are extracted

from the recorded acceleration time series referenced to previous methods (Zeghal et al. 1995; Kamai & Boulanger 2009, Kishida & Tsai 2021). Inversion analyses of V_s profiles are also conducted by computing horizontal Fourier spectrum ratio between downhole to ground surface with genetic algorithm (GA) and simulated annealing (SA) approach (Yamanaka 2007). With the results of these analyses with recorded excess pore water pressure, the insitu dynamic soil properties were investigated by capturing the uncertainties in the resulted V_s profiles.

2 ANALYSED DATA

Strong ground motions are downloaded from Wildlife Liquefaction Site. Figure 1 shows the geological profile and instrumentation layout of Wildlife Liquefaction Array (NEES@UCSB, http://nees.ucsb.edu/data-portal). Figure 2 shows a plan view of the sensor locations. The near-surface soil layer is composed of a 2.5 to 3.0 m-thick silty clay to clayey silt. This layer is underlain by silt, silty sand, and sandy silt layer with a thickness of 3.5–4.0 m and is highly susceptible to soil liquefaction (Bierschwale & Stokoe 1984). A thick silty clay to clay layer underlies the liquefiable sand layer. The instrumentation consists of triaxial accelerometers (Kinemetrics Episensor ES-T) and pressure transducers (Quanterra 330 L) installed at 9 and 10 different locations, respectively. The sensors have sampling rates of 200 Hz. The accelerometers are located at ground surface, and at depths of 2.5, 5.5, 7.7, 30, and 100 m. Locations 01 and 04 are just above and below the liquefiable layer, and locations 02 and 03 are within the liquefiable soil. The pressure transducers are placed at ground surface, and at depths of 2.64, 2.95, 3.28, 3.51, 4.30, 4.42, 4.71, and 6.23 m. Locations 62/63 and 66/67 are installed at the top and the bottom of the liquefiable layer, respectively, and locations 64/65 are at the middle of this layer. Table 1 lists the 13 earthquake events analyzed in this study. Peak ground acceleration (PGA) and hypocenter distance ranged from 0.003 g to 0.31 g and 6.1 km to 350 km, respectively. Moment magnitude (M) ranged from 3.4 to 7.2. The recorded data can be downloaded from NEES@UCSB (http://nees.ucsb.edu/data-portal).

3 ANALYSIS METHOD

Three different approaches are conducted to obtain V_s profiles from the recorded time series. This section describes these approaches.

3.1 *Travel-time approach*

The approach computes the wave travel times between downhole sensors. Elgamal et al. (1995) calculated these by cross-correlation methods (CCMs), whereas Haddadi and Kawakami (1998) analyzed recordings using the normalized input-output method (NIOM). Both methods return the incident and reflected wave travel times, whereas the incident wave velocities are only selected because of the large uncertainties in the reflected waves (e.g. Elgamal et al. 1995, Kishida et al. 2018a) (Figure 3). The approach is reliable when the separation distance is relatively large because the resolutions of the resulted wave velocities depend on the sampling frequency of the recorded signals. The algorithm works from small to large shaking levels. When compression and surface waves are dominant, it will result in unstable V_s estimates. This study rotates the azimuthal angles from 0 to 180 degree by one degree within the same time window. The mean and standard deviations are obtained in natural log scale from these data (Kishida & Tsai 2021).

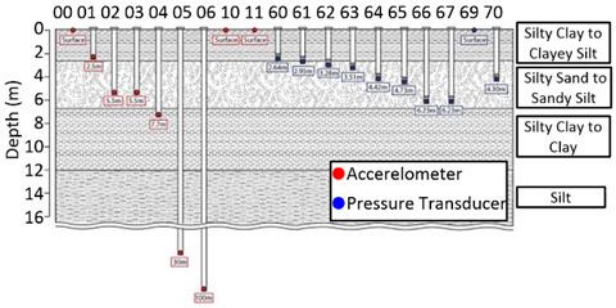

Figure 1. Geological profile and instrumentation layout of the Wildlife Arrays; red and blue dots show accelerometers and pore-water pressure sensors, respectively. Numbers indicate sensor location codes. Depth of soil layers and soil types are shown from the ground level (NEES@UCSB, http://nees.ucsb.edu/data-portal).

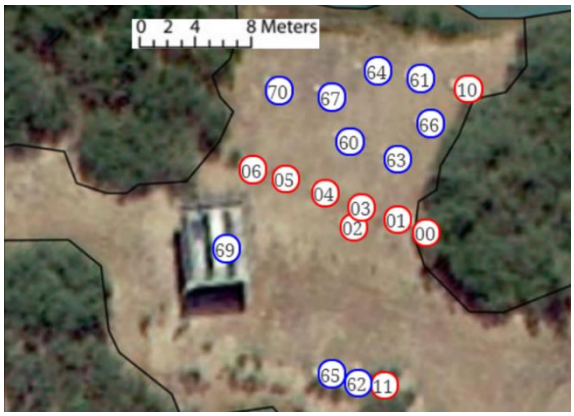

Figure 2. A plan view of the instrumentation layout of the Wildlife Arrays; red and blue dots show accelerometers and pore-water pressure sensors, respectively. (NEES@UCSB, http://nees.ucsb.edu/data-portal).

Table 1. Analyzed earthquake events for Wildlife Liquefaction Arrays

CI Event ID	Origin Time (UTC)	Magnitude (**M**)	Hypocentral distance (km)
14607652	2010-04-04T22:40:43	7.2	94.8
15199681	2012-08-26T19:31:22	5.4	6.1
15200401	2012-08-26T20:57:57	5.5	7.8
15200489	2012-08-26T21:15:29	4.1[1]	11.3
15201537	2012-08-26T23:33:25	4.6[1]	18.2
15202921	2012-08-27T04:41:36	4.5[1]	12.3
15203249	2012-08-27T06:31:27	3.4[2]	12.2
37298672	2014-12-24T05:51:51	4.2	13.2
37166079	2015-05-21T03:15:30	4.1[2]	17.6
37374687	2016-06-10T08:04:39	5.2	93.4
37644544	2016-07-31T16:21:06	4.0	26.6
38443183	2019-07-04T17:33:49	6.4	342.1
38457511	2019-07-06T03:19:53	7.1	352.6

3.2 *Stress-strain approach*

Stress-strain behaviors are inverted using recorded accelerograms. Shear stresses (τ) are calculated between accelerometers by summation of horizontal inertia force of soil from the upper sensor to that point. Accelerations are assumed to vary linearly between accelerometers (Kamai & Boulanger 2009). By integrating the mass multiplied with horizontal acceleration, the time series of τ at the depth are computed.

Shear strain (γ) is computed by differentiating the displacement time series with depth. Kamai & Boulanger (2009) listed several techniques to compute the γ and reported that the performance of weighted residual (Brandenberg et al. 2010) and cubic interpolation techniques are stable. This study calculates the displacement time series following the approach by Kishida

& Tsai (2021) and adopts the algorithm of weighted residual to compute γ time series.

Figure 4 shows the stress-strain behaviors observed at Event 15202921 at the depth of 1.25 and 4 m, respectively, within the time window from 16 – 18 s. By selecting the maximum and minimum τ and γ (red dots), shear modulus (G) is computed by using mean values (blue dots). The computed *G* is converted to V_s by

$$V_S = \sqrt{G/\rho} \quad (1)$$

where ρ is the soil density of 2.0 g/cm^3. The resulted V_s are 61 and 75 m/s at these depths, respectively. This appr oach works well when the separation distances between se nsors are relatively small compared to the wave lengths of the ground motions (e.g. d < $V_s/5f_{max}$, Lysmer et al. 19 75, f_{max} is the maximum interested frequency). However, it s errors increase as distance increases. The V_s are compute d in different azimuthal angles. Mean and standard deviati on are computed within a time window.

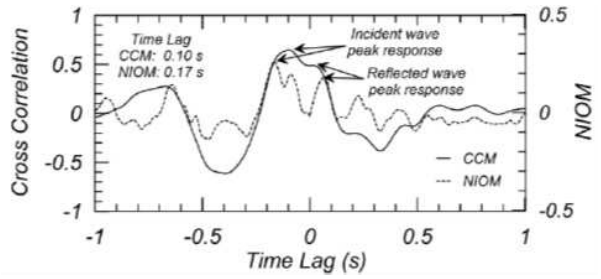

Figure 3. Reponses of CCM and NIOM (Kishida et al. 2018a).

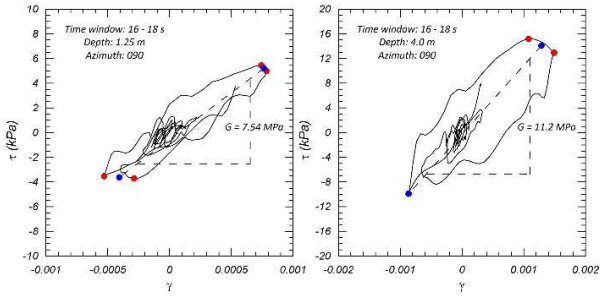

Figure 4. Stress-Strain curve during Event 15202921 with the time window from 16 – 18 s at the depth of (a) 4, and (b) 6.6 m, respectively.

3.3 *Inversion of H/H Ratio*

The recorded time series are windowed to compute ratio of Fourier amplitude spectrum (FAS) for horizontal components between ground surface and downhole sensors (H/H ratio). The window's size was 2.56 s, which corresponds to 512 data points. The dt is the time step of the recorded time series. By rotating the azimuthal angles from 0 to 180, median H/H ratio was computed. Smoothing of FAS is not applied because it would distort its characteristics (Kottke et al. 2018). Inversion analysis was conducted to fit the theoretical transfer function to the observed data. The algorithm follows a combination of GA and SA (Yamanaka 2007) with linear seismic response analyses of horizontally layered soil deposits (e.g. Schnabel et al. 1972). This approach assumes that the recorded signals are dominated by propagation of horizontal shear waves. The results are unstable if the time windows are selected in the P-wave and Coda durations. When substantial softening occurs in soil behaviors, the amplitude of first resonant decreases significantly in H/H ratio; then the theoretical transfer function cannot converge to the observed ones. Hence, there is a limitation of the currently adopted algorithm because it is not applicable to very strong motions. The analysis starts from a pair of sensors at ground surface and the shallowest downhole depth. Seven inversions are performed and the average profile of three best fitted results are stored. Uncertainties of V_s values are also stored. At the next step, a pair of ground surface and second shallowest downhole sensors is selected for inversion analysis to obtain deeper V_s profiles. The V_s profiles from surface to the shallowest downhole sensor is fixed in this stage. By repeating this process, the V_s profiles from ground surface to the depth of 30 m are inverted during strong motions. Figure 5(a) shows the example of H/H ratio between ground surface to the depth of 2.5 m. The profiles that are inverted by fitting the transfer function show the reduction of V_s from ground surface to the depth of 2.5 m (Figure 5b). After fixing the V_s profile from ground surface and 2.5 m, the V_s profiles were inverted in Figure 5(c) and 5(d) from ground surface and 5.5-m depth.

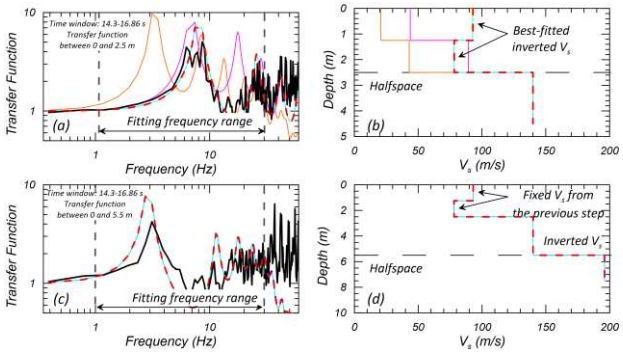

Figure 5. (a) H/H FAS ratio between ground surface to the depth of 2.5 m (b) Inverted V_s profile between ground surface to the depth of 2.5 m, (c) H/H FAS ratio between ground surface to the depth of 5.5 m (d) Inverted V_s profile between ground surface to the depth of 5.5 m.

4 COMPARISON OF INVERTED VS PROFILES

Figure 6 shows the (a) observed times series, (b) pore-water pressure ratio, (c) shear strain, (d) V_s at depth, (e) uncertainties in V_s, respectively, during Event 15202921. The pore-water pressure and shear strain increase sharply with the arrival of S-wave packets at 15 sec. The V_s at shallow profile substantially decreases accordingly. Figure 6(d) shows that the observed V_s are consistent among these different approaches. The time-interval and the stress-strain approaches return the values through the time series. However, the inversion analysis only returns the reliable results during S-wave duration. Figure 6(e) shows that the standard deviations of the travel-time and the stress-strain approaches are consistent with a range of 0.08. On the other hand, that of inversion approach is substantially larger with a range of approximately 0.5.

Figure 7 shows the variation of V_s profiles during strong shakes in Event 15202921. Suspension logging data are also presented (NEES@UCSB, http://nees.ucsb.edu/facilities/wla). Representative profiles are computed by combining the results from different approaches. From ground surface to the depth of 2.5 m (Figure 7a), the V_s from travel-time approach was eliminated because it resulted in substantially larger values with large scattering compared to the stress-strain approach. This observation is due to the fact that the separation distance between sensors are small by which the accuracy of the travel-time approach decreases with the limited sampling frequency. Similarly, from the depth of 7.7 to 18 m (Figure 7d), the V_s from the stress-strain approach was eliminated because it resulted in substantially large standard deviations compared to the travel-time approaches. This observation is due to the fact that the separation distance between the sensors was too large to compute the stress-strain behaviors. After eliminating these

data, the V_s between the sensors are weighted with its inverse of the variance.

Since substantial settlement is expected after the occurrence of soil liquefaction due to the fabric evolution via soil dilatancy process (Ishihara & Yoshimine 1992, Dafalias & Manzari 2004), it is useful to combine reliable measurements of V_s with pore-water pressure measurement. The computation time for the presented approach is reasonably short; hence, it can be adopted to the near real-time monitoring protocol.

5 CONCLUSIONS

Different methodologies to identify the dynamic responses of soils using the data obtained at Wildlife Liquefaction Array are discussed in this study. Here we mainly focused on the comparison and combination of three different methodologies to reduce the uncertainties in dynamic soil behavior during the identification, whereas previous studies primarily focused on developing the methods to analyze downhole data.

Travel time approach is found to be reliable when the separation distance is relatively large, because the resolutions of the resulted shear wave velocities depend upon the sampling frequency of the recorded signals. Shear stress-strain behaviors are computed using the techniques mentioned in Kamai & Boulanger (2009). We observed that stress-strain approach works well when the separation distances between sensors are relatively narrow compared to the wave lengths of the ground motions. However, it resulted in the unreliable V_s value as separation distance increased. The V_s can be computed with different azimuthal angles and reliable results are obtained by averaging these. In the third approach, inversion analysis is conducted to fit the theoretical transfer function to the observed H/H ratio. Seven inversions are conducted and average profiles of three best fitted results are stored along with the uncertainties in the shear wave velocity values.

By comparing these results, travel time approach and stress-strain approach return the values through the time series from p-wave arrival to the end of Coda. However, the inversion analysis only returns the reliable results during the S-wave duration. The standard deviation of the travel time and stress strain approach are observed in the range of 0.08, whereas the standard deviation of the inversion approach is found to be larger, in the range of 0.5. V_s profiles are created by combining the results from these three approaches and displayed that this method provided reliable results that would be useful for monitoring of the structural damages in a near real-time manner.

6 ACKNOWLEDGEMENTS

The analyzed data are provided by NEES@UCSB. The Abu Dhabi Department of Education and Knowledge (ADEK) supported the research through the 2018 ADEK Award for Research Excellence (AARE18-148). Access for the referenced professional journals is granted by Khalifa University of Science and Technology, Abu Dhabi, UAE. The authors appreciate these supports for result presentation. The author also gratefully acknowledge the support from the Ministry of Science and Technology, Taiwan under Award No. 109-2625-M-005 -003

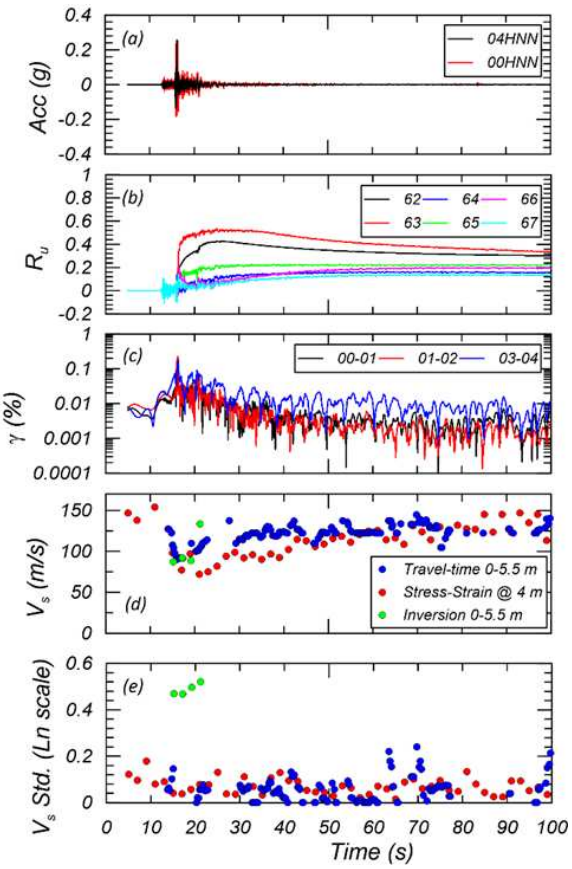

Figure 6. (a) acceleration times series, (b) pore-water pressure ratio, (c) shear strain, (d) V_s time series, (e) uncertainties in V_s during Event 15202921.

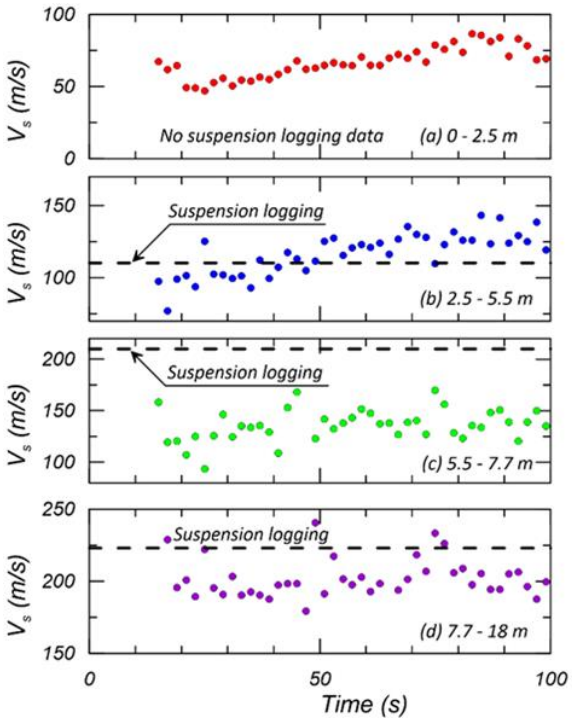

Figure 7. Variation in Vs combined from three different approaches from the depth (a) 0 – 2.5 m, (b) 2.5 – 5.5 m, (c) 5.5 – 7.7 m, (d) 7.7 – 18 m

7 REFERENCES

Aguirre J, Irikura K 1997. Nonlinearity, liquefaction, and velocity variation of soft soil layers in Port Island, Kobe, during the Hyogo-ken Nanbu earthquake. *Bull Seismol Soc Am* 87:1244–1258.

Bierschwale JG Stokoe KHI (1984) Analytical evaluation of liquefaction potential of sands subjected to the 1981 Westmorland earthquake. Geotechnical engineering report GR 84-15, University of Texas, Austin.

Brandenberg, Scott J., Daniel W. Wilson, & Mark M. Rashid 2010. A Weighted Residual Numerical Differentiation Algorithm Applied to Experimental Bending Moment Data. *Journal of Geotechnical and Geoenvironmental Engineering*, 136(6) DOI:10.1061/(ASCE)GT.1943-5606.0000277

Dafalias, Y. & Manzari, M. T. 2004. Simple Plasticity Sand Model Accounting for Fabric Change Effects, J. Eng. Mech., 2004, 130(6): 622-634.

Elgamal AW, Zeghal M, Tang HT, Stepp JC 1995. Lotung downhole seismic array. I: evaluation of site dynamic properties. *J Geotech Eng* 121:350–362.

Haddadi HR, Kawakami H 1998. Modeling wave propagation by using normalized input-output minimization (NIOM) method for multiple linear systems. Doboku Gakkai Ronbunshu 584:29–39.

Hashash YMA, Musgrove MI, Harmon JA, Ilhan O, Xing G, Groholski DR, Phillips CA, Park D 2020. DEEPSOIL 7.0, User manual, Urbana, IL, Board of Trustees of University of Illinois at Urbana-Champaign.

Ishihara, K., & Yoshimine, M., 1992. Evaluation of settlements in sand deposits following liquefaction during earthquakes, *Soils and Foundations* 32(1), 173–88.

Kamai, R. & Boulanger, R.W. 2009, Characterizing localization processes during liquefaction using inverse analyses of instrumentation arrays. *Meso-Scale Shear Physics in Earthquake and Landslide Mechanics*, Y. H. Hatzor, J. Sulem, and I. Vardoulakis, eds., CRC Press, 219-238.

Kishida, T. & Tsai, C.C. 2021. Wave Velocities depending on Shear Strain, Directionality, and Excess Pore Water Pressure from Wildlife Liquefaction Arrays, *Bulletin of Earthquake Engineering*, 19:2371–2388, DOI: 10.1007/s10518-021-01074-4.

Kishida, T., Derakhshan, S., Muin, S., Darragh, B., Bozorgnia, Y., Kuehn, N., and Kwak, D. Y. 2018b, Multivariate Prediction of Moment Magnitude for Small-to-Moderate Magnitude Earthquakes in Iran, Earthquake Spectra, 34(1), February, doi: 10.1193/050917EQS086M.

Kishida, T., Haddadi, H., Darragh, R. B., Kayen, R. E., Silva, W. J., and Bozorgnia Y. 2018a. Apparent Wave Velocity and Site Amplification at the CSMIP Carquinez Bridge Geotechnical Arrays during the 2014 M6.0 South Napa Earthquake, Earthquake Spectra, 34(1), February, doi: 10.1193/042317EQS074M, pp 327–347.

Kottke A, Abrahamson NA, Boore, DM, Bozorgnia Y, Goulet C, Hollenbeck J, Kishida T, Der Kiureghian A, Ktenidou O, Kuehn N, Rathje E, Silva W, Thompson EM. & Wang X. 2018. Selection of random vibration procedures for the NGA-East project. PEER Report 2018 5.

Lysmer, J., Udaka, T., Tsai, C-F, & Seed, H. B., 1975. FLUSH A Computer Program for Approximate 3-D Analysis of Soil-Structure Interaction Problems, Earthquake Engineering Research Center, Report No. EERC 75-30, November 1975.

Schnabel, P. B., Lysmer, J., & Seed, H. B., 1972. SHAKE: A Computer Program for Earth quake Response Analysis of Horizontally Layered Sites. *Report No. UCB/EERC-2/12*, Earthquake Engineering Research Center, University of California, Berkeley, December.

Steidl JH, Civilini F, Seale S 2014. What have we learned after a decade of experiments and monitoring at the NEES@UCSB permanently instrumented field sites?. In: Tenth U.S. national conference on earthquake Engineering frontiers of earthquake engineering, July 21–25, 2014, Anchorage, Alaska.

Yamanaka, H. 2007. Inversion of surface-wave phase velocity using hybrid heuristic search method, *BUTSURI-TANSA,* 60, 265-275, DOI: 10.3124/segj.60.265.

Youd LT, Steidl J, Steller RA 2007. Instrumentation of the Wildlife Liquefaction Array. In: 4th international conference on earthquake geotechnical engineering, Thessaloniki, Greece, June 25–28, 2007; Paper No. 1251.

Zeghal M, Elgamal AW 1994. Analysis of site liquefaction using earthquake records. *J Geotech Eng*, ASCE, 120(6):996–1017.

Zeghal M, Elgamal AW, Tang HT, Stepp JC 1995. Lotung downhole array II: evaluation of soil non-linear properties. J Geotech Eng 121(4):363–378.